BIOCHEMISTRY
including biophysical chemistry & molecular biology

Article

pubs.acs.org/biochemistry

Structural and Biochemical Insights into the Mechanism of Fosfomycin Phosphorylation by Fosfomycin Resistance Kinase FomA

Svetlana Pakhomova,* Sue G. Bartlett, Pamela A. Doerner, and Marcia E. Newcomer

Department of Biological Sciences, Louisiana State University, Baton Rouge, Louisiana 70803, United States

Supporting Information

ABSTRACT: We present here the crystal structures of fosfomycin resistance protein (FomA) complexed with MgATP, with ATP and fosfomycin, with MgADP and fosfomycin vanadate, with MgADP and the product of the enzymatic reaction, fosfomycin monophosphate, and with ADP at 1.87, 1.58, 1.85, 1.57, and 1.85 Å resolution, respectively. Structures of these complexes that approximate different reaction steps allowed us to distinguish the catalytically active conformation of ATP and to reconstruct the model of the MgATP·fosfomycin complex. According to the model, the triphosphate tail of the nucleotide is aligned toward the phosphonate moiety of fosfomycin, in contast to the previously published MgAMPPNP complex, with the attacking fosfomycin oxygen positioned 4 Å from the γ-phosphorus of ATP. Site-directed mutagenesis studies and comparison of these structures with that of homologous *N*-acetyl-L-glutamate and isopentenyl phosphate kinases allowed us to propose a model of phosphorylation of fosfomycin by FomA enzyme. A Mg cation ligates all three phosphate groups of ATP and together with positively charged K216, K9, K18, and H58 participates in the dissipation of negative charge during phosphoryl transfer, indicating that the transferred phosphate group is highly negatively charged, which would be expected for an associative mechanism. K216 polarizes the γ-phosphoryl group of ATP. K9, K18, and H58 participate in stabilization of the transition state. D150 and D208 play organizational roles in catalysis. S148, S149, and T210 participate in fosfomycin binding, with T210 being crucial for catalysis. Hence, it appears that as in the homologous enzymes, FomA-catalyzed phosphoryl transfer takes place by an in-line predominantly associative mechanism.

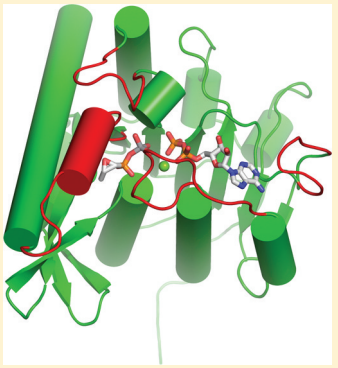

Antibiotic resistance is a continuously emerging problem that poses a significant threat to global public health. Many previously known "miracle" drugs have lost their effectiveness against bacteria. On the other hand, very few new antimicrobial agents are brought to the market. Rather than searching for new antimicrobial agents, researchers in the field of drug discovery have emphasized the development of new improved formulations, more effective delivery systems, and understanding of resistance mechanisms. A comprehensive understanding of the resistance mechanism is a key requirement in the drug discovery process. Such knowledge can be exploited in designing inhibitors that can be effective against antibiotic resistance.

Fosfomycin (*cis*-1,2-epoxypropylphosphonic acid) (Scheme 1) is a common broad-spectrum antibiotic successfully used to treat urinary tract infections. Its mode of action is based on the inhibition of the enzyme UDP-*N*-acetylglucosamine-3-*O*-enolpyruvyl transferase, which is responsible for the first stage of peptidoglycan biosynthesis.[1] Fosfomycin is considered to be a somewhat "old" drug because it has been prescribed in clinical practice since 1969.[2,3] Nevertheless, it is still the only drug approved by the Food and Drug Administration for treatment of acute cystitis during pregnancy.[4] Successful application of the antibiotic for treatment of multidrug-resistant Gram-positive and Gram-negative bacterial infections in combination with other antibiotics has recently been reported,[5] which prompted further evaluation of its potential clinical effectiveness, especially in cases involving multidrug-resistant pathogens in which previous antibiotics have failed to cure the infection.

Scheme 1. Enzymatic Reactions Catalyzed by FomA and FomB Proteins

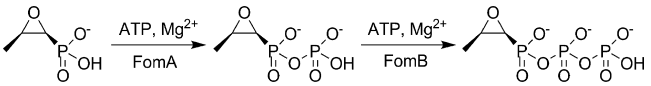

One of the most attractive features of fosfomycin is the chemical stability of the molecule. The combination of a carbon−phosphorus bond in conjunction with the epoxide ring makes the molecule extremely stable. It has almost no toxicity in humans,[2] is eliminated in the kidneys in its active form without metabolites, and can be dialyzed. However, several fosfomycin resistance proteins, namely, FosA, FosB, FosC, and FosX, that inactivate the antibiotic by different mechanisms are

Received: March 23, 2011
Revised: July 5, 2011
Published: July 5, 2011

Table 1. Data Collection, Phasing, and Refinement Statistics

	MgATP	ATP·fosfomycin	MgADP·$FMVO_3$	MgADP·FM	ADP
wavelength (Å)	1.38079	1.38079	1.38079	1.38079	1.38079
resolution (Å)	1.87	1.58	1.85	1.57	1.85
temp (K)	100	100	100	100	100
space group	$P3_221$	$P3_221$	$P3_221$	$P3_221$	$P3_221$
cell dimensions					
a (Å)	85.88	87.33	87.38	87.91	87.67
c (Å)	80.15	78.54	79.00	79.23	78.89
no. of molecules per asymmetric unit	1	1	1	1	1
no. of unique reflections	26774	42575	29919	47552	30430
R_{sym}[a,b] (%)	3.6 (45.4)	3.9 (56.1)	4.6 (70.5)	3.5 (45.9)	10.6 (53.9)
completeness[a] (%)	93.4 (96.9)	89.0 (88.9)	99.3 (99.3)	95.6 (85.0)	98.6 (93.2)
redundancy[a]	2.9 (2.4)	4.4 (4.2)	4.9 (4.0)	2.4 (2.1)	3.6 (3.4)
$I/\sigma(I)$[a]	32.0 (1.9)	35.6 (1.8)	31.4 (1.7)	25.0 (1.5)	12.3 (1.6)
		Refinement Statistics			
resolution range (Å)	23.01−1.87	26.86−1.58	27.32−1.85	35.14−1.57	34.21−1.85
no. of reflections used in refinement	24958	39740	27413	43681	27860
σ cutoff used in refinement	none	none	none	none	none
R/R_{free}[c] (%)	18.49/20.54	16.14/20.29	16.41/21.94	15.68/17.17	16.50/21.33
no. of refined atoms					
protein	1904	2044	2092	1928	1963
heterogen atoms	38	39	40	40	27
water	108	203	136	232	169
average *B* factor (Å^2)					
protein	39.3	31.3	41.5	31.3	35.9
water	47.5	33.2	34.7	35.7	35.0
nucleotide	47.6	46.4	45.0	44.8	48.7
fosfomycin	–	29.3	38.8 ($FMVO_3$)	50.9 (FM)	–
magnesium	59.9	–	43.3	57.2	–
root-mean-square deviation					
bonds (Å)	0.018	0.023	0.022	0.023	0.023
angles (deg)	1.763	2.113	2.002	2.154	2.044
ML estimated coordinates errors (Å)	0.082	0.045	0.081	0.042	0.070
Ramachandran plot (%)[d]					
favored	96.7	98.5	96.0	98.3	96.5
allowed	3.3	1.5	4.0	1.7	3.5
generous	0	0	0	0	0
disallowed	0	0	0	0	0

[a]Values in parentheses are for the highest-resolution shell. [b]$R_{sym} = \sum|I_i - \langle I_i\rangle|/\sum I_i$, where I_i is the intensity of the *i*th observation and $\langle I_i\rangle$ is the mean intensity of the reflection. [c]$R = \sum||F_o| - |F_c||/\sum|F_o|$, where F_o and F_c are the observed and calculated structure factor amplitudes, respectively. R_{free} is calculated using 1.6, 1.5, 1.5, 1.5, and 1.5% of the reflections omitted from the refinement for the MgATP, ATP·fosfomycin, MgADP·$FMVO_3$, MgADP·FM, and ADP structures, respectively. The same R_{free} set was used in every case because of the isomorphous character of the data sets. [d]Molprobity validation.

described in the literature.[6−9] Fosfomycin resistance kinases FomA and FomB are the newest representatives of the class of fosfomycin resistance proteins.[10,11] Together, these novel enzymes inactivate fosfomycin by phosphorylation of the antibiotic's phosphonate group (Scheme 1).

We previously described the high-resolution crystal structure of fosfomycin resistance protein FomA from *Streptomyces wedmorensis* in a complex with diphosphate (DPO) and in a ternary complex with MgAMPPNP and fosfomycin (MgAMPPNP·fosfomycin) at 1.53 and 2.2 Å resolution, respectively.[12] The structures revealed the molecular fold of the protein, which classifies it among the members of the amino acid kinase (AAK) superfamily of enzymes, identified the active site residues of FomA that could be responsible for substrate binding and specificity, and elucidated their proposed roles in catalysis. A high degree of similarity in molecular fold as well as in the organization of the active sites was observed between FomA and the *N*-acetyl-L-glutamate kinase (NAGK), for which the catalytic reaction is well studied and proceeds via the associative in-line mechanism.[13] However, the ternary complexes of the two enzymes, which superimpose well with respect to substrates and catalytic residues K9, K216, and D150 (FomA numbering), show different orientations of the γ-phosphates of the nucleotide molecules. In addition, the triphosphate tail of AMPPNP is not aligned toward the phosphonate group of fosfomycin, and the shortest distance

between oxygen atoms of the phosphonate group of fosfomycin and the phosphorus atom of AMPPNP is 5.19 Å, a value that is too long for the optimal in-line phosphoryl transfer reaction. Such observations suggested that the FomA-catalyzed reaction may proceed by a mechanism different from that observed for NAGK, or the catalytic conformation of ATP may be significantly different from the one observed for AMPPNP in the MgAMPPNP·fosfomycin crystal structure. To address these questions, we determined crystal structures of additional ternary complexes of FomA that provide an approximation of different reaction steps: with MgATP (MgATP), with ATP and fosfomycin (ATP·fosfomycin), with MgADP and fosfomycin vanadate (MgADP·$FMVO_3$), with MgADP and the product of the enzymatic reaction, fosfomycin monophosphate (MgADP·FM), and with ADP (ADP). Site-directed mutagenesis studies presented here helped to determine the role of different active site residues in catalysis.

EXPERIMENTAL PROCEDURES

Chemicals and Materials. Fosfomycin monophosphate was enzymatically synthesized, purified, and kindly provided by T. Kuzuyama (The University of Tokyo, Tokyo, Japan). All other chemicals were purchased from Sigma/Fluka at the highest grade available.

Protein Preparation and Crystallization. Protein was expressed and purified according to the published procedure.[12] Studied complexes have been obtained by soaking FomA crystals grown as described previously[12] in modified mother liquor for at least 30 min prior to the collection of data. The compositions of soaking solutions were as follows: 17% PEG 3350, 15% glycerol, 0.1 M MES (pH 5.5), 10 mM ATP, and 10 mM $MgCl_2$ (MgATP complex); 17% PEG 3350, 25% glycerol, 0.1 M MES (pH 7.1), 10 mM ATP, and 10 mM fosfomycin (ATP·fosfomycin complex); 17% PEG 3350, 25% glycerol, 0.1 M MES (pH 7.0), 10 mM ADP, 50 mM $MgCl_2$, 10 mM fosfomycin, and 10 mM $NaVO_3$ (MgADP·$FMVO_3$ complex); 17% PEG 3350, 25% glycerol, 0.1 M MES (pH 7.0), 10 mM ADP, 50 mM $MgCl_2$, and 10 mM fosfomycin monophosphate (MgADP·FM complex); and 17% PEG 3350, 25% glycerol, 0.1 M MES (pH 7.0), 10 mM ADP, and 50 mM $MgCl_2$ (ADP complex).

Data Collection. Diffraction data were collected at 100 K at the PX station at the Center for Advanced Microstructures and Devices at Louisiana State University with a MAR charge-coupled device camera. Data were processed with HKL2000.[14] Data collection and data processing statistics are listed in Table 1.

Determination of Crystal Structures. The molecular replacement procedure (MR) was applied to locate a solution. A monomer of FomA from the FomA·MgAMPPNP·fosfomycin ternary complex (Protein Data Bank entry 3D41) was used as a search model. The positioned MR models were refined using the maximum likelihood refinement in REFMAC[15] with the TLS parameters generated by the TLSMD server.[16] TLS tensors were analyzed, and anisotropic *B* factors were derived with TLSANL.[17] O[18] was used for model building throughout the refinement. Details of refinement of each particular complex follow.

MgATP Complex. The presence of ATP and Mg^{2+} cation was confirmed by difference Fourier. One glycerol molecule was modeled in the active site according to the electron density shape. Nine residues (residues −8 to 0) of the N-terminal poly-His tag were visible and were modeled into the electron density. The final model consists of protein residues −8 to 56, 70−178, 182−202, and 211−262. Alternate conformations have been built for residues M1, L6, L115, R116, S117, and Q118. A total 108 water molecules have been added to the final model.

ATP·Fosfomycin Complex. The final model consists of protein residues −11 to 177, 183−205, and 212−264, one ATP, one fosfomycin, and 203 water molecules. Alternate conformations have been built for protein residues L6, I8, Y43, V82, and C106.

MgADP·$FMVO_3$ Complex. The final model consists of protein residues −11 to 262, one ADP molecule, one Mg^{2+} cation, one fosfomycin vanadate, and 136 water molecules. Alternate conformations have been built for protein residues L6, I8, Y43, C106, and E161.

MgADP·FM Complex. The final model consists of protein residues −8 to 55, 69−178, 183−205, and 211−262, one ADP molecule, one Mg^{2+} cation, one fosfomycin monophosphate, and 232 water molecules. Alternate conformations have been built for protein residues L6, I8, Y43, C106, L115, S193, and R226.

ADP Complex. The final model consists of protein residues −8 to 62, 68−204, and 211−262, one ADP molecule, and 169 water molecules. Despite the fact that the soaking solution contained a high concentration of $MgCl_2$, no electron density that could be attributed to Mg^{2+} cations was observed in the active site. Alternate conformations have been built for amino acid residues L6, I8, Y43, and C106.

Generation of S148A, S149A, T210A, H58L, K9A, K18A, and D208A Mutants. Mutants were created using whole plasmid PCR and Pfu UltraII polymerase (Stratagene) as described previously.[19] All mutant enzymes were expressed in bacteria as soluble proteins in yields comparable to that of the wild-type enzyme. They were isolated and purified essentially as described for the native protein.

Kinetic Studies. Kinetic measurements for wild-type FomA and all site-specific FomA mutants were performed at 25 °C using the pyruvate kinase−lactate dehydrogenase coupled assay.[10] The reaction mixture in a volume of 1 mL contained 4.6 units of pyruvate kinase, 6.6 units of lactate dehydrogenase, 100 mM sodium HEPES buffer (pH 7.2), 10 mM $MgCl_2$, 0.3 mM NADH, 1 mM phosphoenolpyruvate (PEP), 100 mM KCl, and several concentrations of fosfomycin and ATP. The reaction rate was measured for 15 min. The K_m for fosfomycin was determined using an enzyme assay system containing 1 mM Na_2ATP^{2-} and various concentrations of fosfomycin. The reaction was initiated by the addition of purified FomA (18 μg) or FomA mutants (107 and 193 μg for S148A and S149A mutants, respectively). Reaction volumes of 170 μL and 287 μg of K9A or 630 μg of D208A in an assay were used to measure kinetic data in the case of the K9A and D208A mutants. Data were analyzed with curve fitting in Sigmaplot. The K_m for Na_2ATP^{2-} was determined using an enzyme assay system containing 1 mM fosfomycin and various Na_2ATP^{2-} concentrations. The reaction was initiated by the addition of the same amount of purified FomA or FomA mutants as in

the case of the determination of the K_m for fosfomycin. Data were analyzed as stated above for fosfomycin.

Figures. All figures of structures were made using PYMOL.[20]

RESULTS

Overall Fold. Five crystalline FomA complexes presented here and two previously reported[12] MgAMPPNP·fosfomycin and DPO structures are isomorphous and exhibit the same overall open $\alpha\beta\alpha$ sandwich polypeptide fold (Figure 1). The

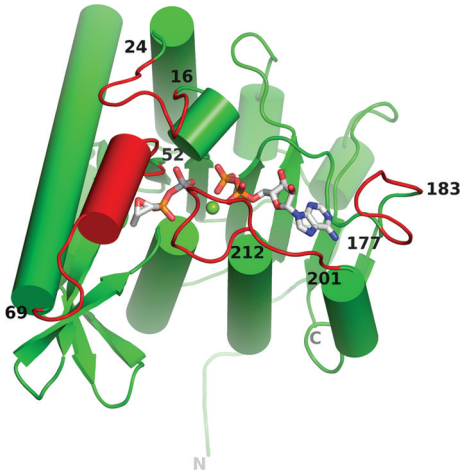

Figure 1. Cartoon representation of a monomer of FomA as it is seen in the MgADP·$FMVO_3$ complex. Ligand molecules are shown as sticks, and Mg^{2+} is shown as a green sphere. Flexible parts of the protein molecule are colored red.

root-mean-square deviations (rmsd) for the equivalent CA atoms between all the structures are less than 1 Å. The enzyme molecules in different complexes show conformational flexibility in four different parts, all of which surround the active site (Figure 1 and Table 1 of the Supporting Information). The loop consisting of residues 16−24 is highly flexible and adopts different conformations in the structures. This loop contains K18, an amino acid residue that was proposed to be important for the catalysis because it forms a hydrogen bond between the NZ atom and a nonbridging oxygen atom of the γ-phosphoryl group of ATP in the MgAMPPNP·fosfomycin complex. Similar H-bonding is also observed in the ATP·fosfomycin complex. The rest of the FomA complexes lack this H-bond. In the MgATP complex, the loop adopts a notably different conformation, turning away from the active site such that K18 (CA) moves up approximately 5 Å in comparison to all the other complexes and is no longer part of the active site.

Residues 52−69 are mostly disordered in the DPO, MgATP, and MgADP·FM complexes (no electron density observed), while they are ordered in the MgAMPPNP·fosfomycin, MgADP·$FMVO_3$, and ATP·fosfomycin structures where they participate in the formation of helix α2 (residues 53−64). The binding of fosfomycin or fosfomycin vanadate appears to be necessary for the ordering of this part of the protein molecule. However, this portion of the molecule is disordered in the MgADP·FM structure despite the fact that the fosfomycin binding site is occupied by the product of the reaction, fosfomycin monophosphate. Such disorder could be explained by the fact that residues 52−69 could also participate in product release.

The loop of residues 177−183, which is basically covering the adenine ring of ATP, is usually very disordered. It has defined electron density only in the MgADP·$FMVO_3$ and ADP complexes.

The segment of amino acid residues 201−212 extends through the entire active site (Figure 1) and is usually not visible in electron density maps. The MgAMPPNP·fosfomycin and MgADP·$FMVO_3$ structures are the only complexes in which this part of the enzyme molecule is ordered. However, amino acid residues 203−211 adopt somewhat different positions. The ordering of the segment of residues 201−212 is in agreement with the ordering of the segment of residues 52−69 of the protein molecule provided that Mg^{2+} is bound. The corresponding part is also disordered in all known crystal structures of isopentenyl phosphate kinases (IPKs). Residues 201−208 essentially cover the nucleotide binding site. There is a notable difference in the conformation of residue W202 between different complexes. W202 is a part of helix α6 (amino acids 195−203) in the DPO, ATP·fosfomycin, MgADP·FM, and ADP complexes and points away from the active site. However, helix α6 becomes broken at amino acid 200 in the MgADP·$FMVO_3$, MgAMPPNP·fosfomycin, and MgATP crystal structures so that W202 moves closer to the nucleotide binding site and participates in stacking interactions with the adenine ring of a nucleotide (Figure 2A,C), hence closing the nucleotide binding site and preparing the enzyme for the reaction. The remainder of the amino acid residues (residues 209−212) are in the proximity of the fosfomycin binding site. The hydroxyl group of T210 directly participates in fosfomycin binding via a hydrogen bond to O3 of the phosphonate moiety of fosfomycin as it is seen in the MgAMPPNP·fosfomycin and MgADP·$FMVO_3$ complexes (Figure 2C). As discussed later, T210 is also crucial for catalysis.

MgATP Complex. The biggest difference between the MgATP and MgAMPPNP·fosfomycin complexes is observed in the orientation of the γ-phosphoryl group of the nucleotides. In the MgATP structure, it is positioned closer to the fosfomycin binding site (Figure 2A). This conformation is fixed by two hydrogen bonds between nonbridging oxygen atoms of the γ-phosphoryl group of ATP and the side chain nitrogen of K9 and the main chain nitrogen of G12, which are not observed in the latter structure. There is also a 2.74 Å hydrogen bond between O1G of the γ-phosphoryl group of ATP and the hydroxyl group of glycerol (3.7 Å to P_γ). The oxygen from the hydroxyl group of glycerol mimics the position of the attacking oxygen of the phosphonate group of fosfomycin. The $O_{\beta\gamma}-P_\gamma-O_{glycerol}$ angle is 154.8°. The Mg^{2+} cation is five-coordinated and is chelated by the nonbridging oxygen atoms of the α-, β-, and γ-phosphate groups of ATP (2.18, 2.82, and 2.18 Å, respectively), a hydroxyl group of glycerol (2.92 Å), and one water molecule (3.12 Å). Extensive disorder of the protein molecule is observed around the fosfomycin binding site, which results in wide-open access to the binding site. The adenine moiety of ATP makes stacking interactions with the side chain of W202 as it does in the MgAMPPNP·fosfomycin complex.

ATP·Fosfomycin Complex. Despite the fact that this crystal structure does not contain Mg^{2+}, the ATP conformation and the system of hydrogen bonds are

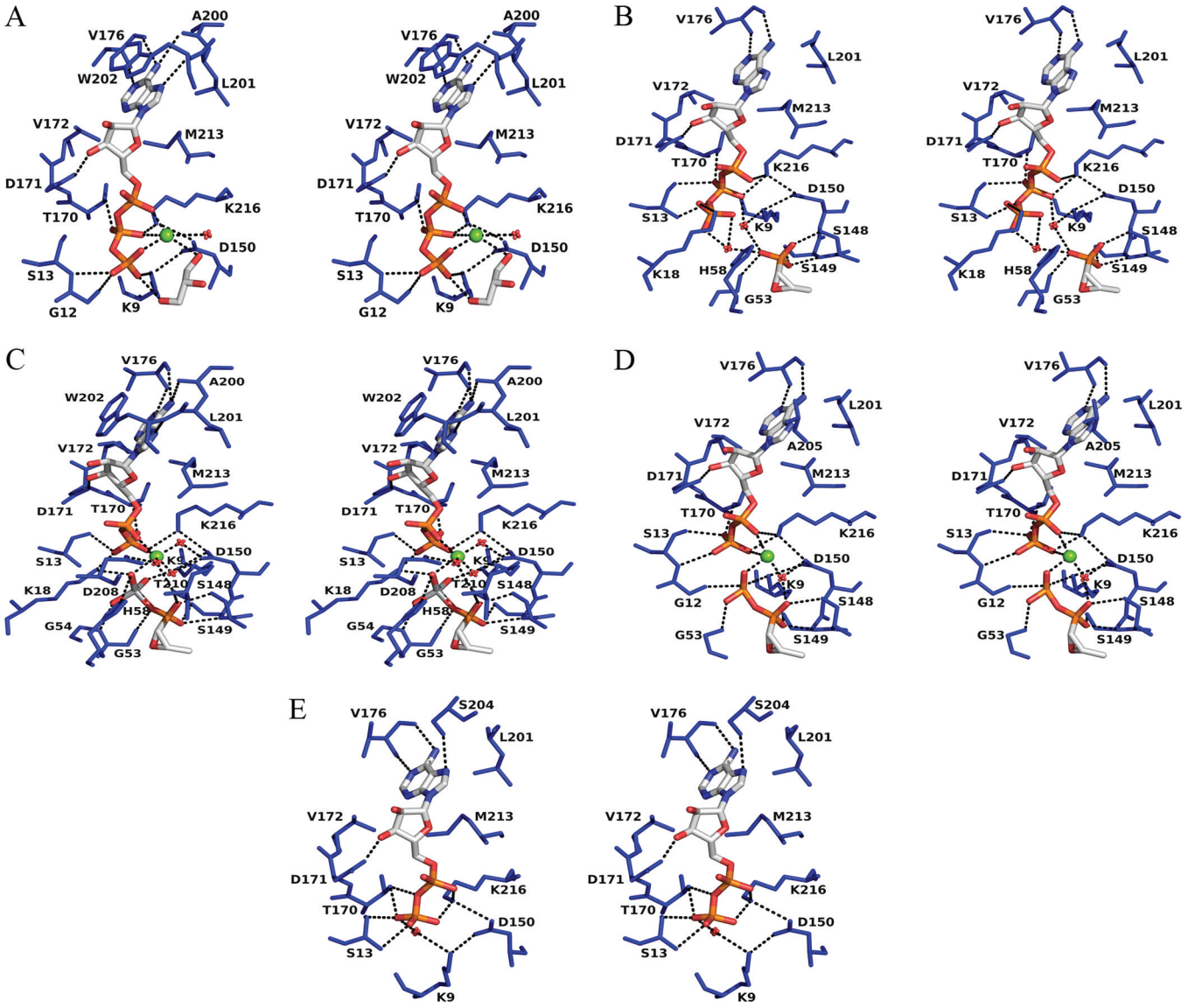

Figure 2. Stereoviews of the active sites in (A) MgATP, (B) ATP·fosfomycin, (C) MgADP·$FMVO_3$, (D) MgADP·FM, and (E) ADP complexes. The ligand molecules are shown as sticks, Mg^{2+} atoms as spheres, and water molecules as crosses, and the interacting protein residues are colored blue.

basically the same as those observed for the AMPPNP molecule in the MgAMPPNP·fosfomycin complex (Figure 2B). The only differences between the two structures are that W202 in the former complex no longer makes stacking interactions with the adenine ring of the nucleotide and that the segment of amino acid residues 206−211, which is adjacent to the magnesium binding site, is disordered with no clear electron density. There is an active site water molecule that mimics the position of one oxygen atom of the γ-phosphate group of ATP in the MgATP complex.

MgADP·$FMVO_3$ Complex. This complex represents the least disordered and the most complete FomA structure. It is the only structure of the five structures reported here with an ordered K9, K18, K216 lysine triangle. The lysine triangle is also ordered in the MgAMPPNP·fosfomycin crystal structure reported previously.[12] However, as will be discussed later, the nucleotide conformation in that structure does not represent the active one and thus is not mechanistically significant. The bond lengths observed indicate that vanadate is covalently bound to the attacking oxygen atom of the phosphonate group of fosfomycin. Hence, fosfomycin vanadate mimics the product of the reaction, fosfomycin monophosphate, and not the transition intermediate. D150 not only coordinates catalytic residues K216 and K9 through salt bridges but also makes H-bonds to two water molecules from the Mg coordination sphere. Magnesium is in the ideal six-coordination state and is chelated by nonbridging oxygen atoms of the α- and β-phosphate groups of ATP (2.15 and 2.12 Å, respectively), one oxygen atom of fosfomycin vanadate (2.36 Å), and three water molecules (1.96, 2.02, and 2.08 Å). The adenine ring of ADP is covered by the side chain of W202 by means of stacking interactions. The side chain nitrogen of K18 forms H-bonds with one oxygen of vanadate of fosfomycin vanadate and one nonbridging oxygen of the β-phosphoryl group of ADP (Figure 2C). The side chain nitrogen of K9 is coordinated with another oxygen of the vanadate moiety. The same vanadate oxygen is also H-bonded with Nε2 of H58. Thus, K9, K18, and H58 are the only residues directly involved in interactions with

dx.doi.org/10.1021/bi2004334|*Biochemistry* 2011, 50, 6909−6919

the vanadate moiety of fosfomycin vanadate, and most likely, these positively charged amino acid residues directly participate in the stabilization of the transition state.

MgADP·FM Complex. The structure is significantly disordered in the active site region. There is no electron density for residues 56−68, 179−182, and 207−210, all of which cover the active site in the MgADP·$FMVO_3$ complex. Amino acid residue K18 does not have defined electron density for the side chain. There is a water molecule in the place of NZ of K18 in the MgADP·VO_3 complex. The glycine rich loop of residues 53−57 is positioned differently compared to that observed in the MgADP·$FMVO_3$ structure, placing residue G54 away from the active site as in the DPO complex. No stacking interactions between the side chain of W202 and the adenine ring of ADP are observed. Mg^{2+} is only four-coordinated [2.19 Å from one oxygen of the phosphate group of fosfomycin monophosphate, 2.17 and 2.67 Å from nonbridging oxygen atoms of the α- and β-phosphate groups of ADP, respectively, and 2.07 Å from a water molecule (Figure 2D)].

ADP Complex. This structure is very similar to that of the MgADP·FM complex. The active side is wide-open because of the extensive disorder of protein loops surrounding it. There are no stacking interactions between the side chain of W202 and the adenine ring of ADP (Figure 2E). The space occupied by the NZ atom of K18 in the MgADP·$FMVO_3$ complex is occupied by a water molecule as in the MgADP·FM complex.

Characterization of FomA Mutants. The previously reported MgAMPPNP·fosfomycin structure[12] identified K18, H58, and D208 as possible catalytic residues in addition to the counterparts of NAGK's catalytic residues K9, K216, and D150. S148, S149, and T210 are residues that participate in fosfomycin binding. We have performed site-directed mutagenesis studies to improve our understanding of the roles of these amino acids in the phosphorylation of fosfomycin by FomA. S148A, S149A, T210A, H58L, K18A, K9A, and D208A FomA mutants were expressed and kinetically characterized (Table 2).

Table 2. Kinetic Data for Wild-Type FomA and FomA Mutants

	K_m^{fos} (μM)	K_m^{ATP} (μM)	k_{cat} (s^{-1})
wild type	9.9 ± 0.7	12.8 ± 1.05	155.9 ± 1.5
S148A	169.8 ± 22.2	42.2 ± 4.2	35.0 ± 2.6
S149A	383.2 ± 45.3	75.5 ± 5.5	14.5 ± 2.2
T210A	ND[a]	ND[a]	–
K9A	23.1 ± 3.1	89.9 ± 11.4	4.5 ± 0.3
K18A	ND[a]	ND[a]	–
H58L	ND[a]	ND[a]	–
D208A	17.5 ± 2.5	60.7 ± 5.1	11.9 ± 0.4

[a]No activity detected.

Nucleotide Binding Site. K9, K216, and D150 correspond to K8, K217, and D162, respectively, in NAGK. In NAGK, K8 and K217 are centrally involved in phosphoryl transfer. K8 stabilizes the transition state by abstracting a developing negative charge, while K217 polarizes the γ-phosphoryl group of ATP. D162 makes salt bridges with both K8 and K217. A D162E mutation shows a 1000-fold decrease in V_m,[21] consistent with the suggestion that D162 organizes catalytic residues K8 and K217. A similar structural feature is found in the FomA protein (K9, K216, and D150 amino acids). Although we did not test the influence of K216 and D150 mutations on the kinetic parameters of the FomA reaction, the strong structural correlation with NAGK and other members of the AAK superfamily of enzymes suggests that D150 plays a similar organizing role in the FomA-catalyzed reaction while K216 likely participates in polarization of the γ-phosphoryl group of ATP. D150 and D208 also belong to the outer coordination sphere of the Mg cation, making strong hydrogen bonds to magnesium-coordinated water molecules in the MgADP·$FMVO_3$ [H-bonds to two water molecules and one water molecule for D150 and D208, respectively (Figure 2C)], MgAMPPNP·fosfomycin (one H-bond each for D150 and D208), and MgADP·FM (H-bond to one water molecule only for D150) complexes. Such an observation could suggest that D150 and D208 also participate in stabilization of the Mg coordination sphere, which in turn organizes the phosphate chain of ATP for phosphoryl transfer. Indeed, the D208A mutation showed a substantial (~15-fold) decrease in k_{cat} (Table 2), suggesting that D208 could participate in such stabilization. Sequence alignment of FomA with IPKs showed that all the IPKs have conserved this aspartate residue. However, all known crystal structures of IPKs have that part of the protein molecule disordered and do not allow structural analysis of this particular aspartate residue.

According to the crystal structures of FomA complexes, K9 accompanies the γ-phosphoryl group of ATP during the phosphoryl transfer. Its NZ group is H-bonded to the γ-phosphate of ATP in the MgATP complex (Figure 2A), one oxygen atom of the vanadate moiety in the MgADP·$FMVO_3$ complex (Figure 2C), and one oxygen of the phosphate group of fosfomycin monophosphate in the MgADP·FM complex (Figure 2D). The corresponding residue in NAGK (K8) was proposed to participate in the stabilization of the transition state. The K9A mutation in FomA showed an ~40-fold decrease in the k_{cat} value, indicating that this residue is indeed important for catalysis.

Structural data for the MgAMPPNP·fosfomycin complex[12] suggested the possible involvement of the positive charge of the side chain of K18 in the catalysis of phosphoryl group transfer. The NZ group of K18 is hydrogen bonded to the nonbridging oxygen atom of the γ-phosphoryl group of ATP in the ATP·fosfomycin (Figure 2B) and MgAMPPNP·fosfomycin complexes. However, as we will discuss below, the nucleotide conformations in these two complexes do not represent the active one. Hence, such an interaction is most likely irrelevant for catalysis. In the MgADP·$FMVO_3$ structure, however, the NZ group of K18 is hydrogen bonded to both a nonbridging oxygen atom of the β-phosphoryl group of ADP and an oxygen atom of the vanadate moiety of fosfomycin vanadate (Figure 2C). Moreover, this residue is not visible at all in the MgATP, MgADP·FM, and ADP complexes. A K18A mutation resulted in an inactivated enzyme. Hence, structural and kinetic data suggest that K18 most likely participates in transition state stabilization.

In the MgAMPPNP·fosfomycin structure, H58 was found virtually at the midpoint of the phosphoryl transfer site in the proximity of both the fosfomycin (3.83 Å) and AMPPNP molecule (3.45 Å), suggesting that H58 could contribute to catalysis. Moreover, this residue is also conserved in all IPKs. Kinetic studies using different mutants in MJ IPK have shown

that this histidine residue plays an essential role in catalysis through hydrogen bond stabilization of the transition state accompanying the nucleophilic displacement of ADP.[22] H60A and H60N mutants completely lose their enzymatic activity, while the H60Q mutant still shows measurable activity. In all known crystal structures of IPKs, this histidine residue makes a hydrogen bond with the terminal phosphates of the substrate isopentenyl monophosphate or the product isopentenyl diphosphate.

H58 is visible only in the MgAMPPNP·fosfomycin, ATP·fosfomycin, and MgADP·$FMVO_3$ FomA complexes (first two complexes have catalytically irrelevant nucleotide conformations, though). In the MgADP·$FMVO_3$ structure, H58 is hydrogen bonded to one oxygen atom of the vanadate moiety of fosfomycin vanadate (Figure 2C). An H58L mutation abolished the catalytic activity of FomA, confirming that this residue is crucial for catalysis. On the basis of kinetic and structural data, we conclude that H58 participates in the stabilization of the transition state of the FomA-catalyzed reaction as in the case of H60 in IPKs.

Fosfomycin Binding Site. The MgAMPPNP·fosfomycin complex showed that three amino acid residues (S148, S149, and T210) hold the substrate fosfomycin in place by hydrogen bonds to the nonattacking phosphonate oxygens of fosfomycin.[12] The increases in K_m^{fos} values associated with the S148A and S149A mutations (~17- and 38-fold increases, respectively) strongly suggest that these mutations hamper fosfomycin binding. All known IPKs have an invariant serine residue at the same position as S148 in FomA. The replacement of T210 with alanine caused essentially a total loss of enzymatic activity (Table 2), indicating that T210 is crucial for the catalysis. T210 is visible only in the MgAMPPNP·fosfomycin and MgADP·$FMVO_3$ complexes, suggesting that this residue most likely participates in transition state stabilization. T210 also belongs to the outer magnesium coordination sphere and makes a strong hydrogen bond (according to the bond length and geometry) to one water molecule. Hence, it could play an organizing role in catalysis, as well.

Although enzymes of the carboxylate division of the AAK superfamily do not have residues that could align with the segment of residues 203–211 of FomA, the recent crystal structure of carbamate kinase (CK) from *Enterococcus faecalis*[23] showed that the side chain of K128 superimposes very well onto T210 of FomA. K128 belongs to the flexible protruding subdomain that hangs over the active site and is an exclusive feature of CKs. A K128A mutation resulted in a very large decrease in k_{cat} and an increase in K_m^{CP} (~2000- and ~600-fold, respectively, relative to those of the wild-type enzyme in identical assays). On the basis of their data, the authors suggested that K128 in CKs most likely participates in substrate–product binding and transition state stabilization, the same role that has been proposed for T210 in FomA. However, in contrast to T210 in FomA, the positively charged side chain of K128 could also participate in withdrawal of the negative charge from carbamoyl phosphate and/or in a neutralization of the negative charge on the γ-phosphate of ATP.

DISCUSSION

Our comparative analysis is based on crystal structures of seven FomA complexes that approximate different reaction steps of the FomA-catalyzed enzymatic reaction. The DPO complex could be considered as a ground state when none of the required substrates is bound in the active site of the enzyme. The MgATP and ATP·fosfomycin complexes may represent the early stages of the reaction in which only two of three necessary reaction components (ATP, fosfomycin, and Mg^{2+} cation) are present. The MgAMPPNP·fosfomycin complex may approximate the next reaction stage at which all the substrates are bound and the reaction is ready to proceed. However, AMPPNP is an inert ATP analogue. Hence, the catalytic conformation of ATP is not necessarily the one observed in the MgAMPPNP·fosfomycin complex. A pentacoordinate transition state complex is considered to be the approximation of the midway reaction stage for the SN_2-type nucleophilic reactions. It has been shown[24−26] that aluminum fluoride, vanadate, or nitrate ions can successfully be used to mimic the γ-phosphoryl group in the catalytic transition state. Our efforts to obtain transition state analogue complexes with either the aluminum fluoride or nitrate ion proved fruitless. Neither AlF_3 nor NO_3^- binds in the active site of the enzyme. Inclusion of $NaVO_3$ in the soaking solution resulted in the crystal complex in which vanadate covalently binds to the fosfomycin, forming fosfomycin vanadate. Such a complex with four-coordinate vanadate mimics the product of the reaction rather than the transition state analogue. The MgADP·FM and ADP complexes represent the final reaction steps. (1) The MgADP·FM complex shows the enzymatic reaction is complete. (2) The ADP complex shows the reaction is complete and the product is released.

Fosfomycin Resistance Kinase versus Isopentenyl Phosphate Kinases. Members of the AAK superfamily of enzymes phosphorylate carboxylate, carbamate, phosphonate, or phosphate functional groups using ATP and Mg^{2+}. The superfamily is divided into two subdivisions according to the nature of the phosphorylated group: the carboxylate subdivision and the phosphate subdivision. The known members of the carboxylate subdivision are carbamate kinase (CK),[27] the N-terminal domain of aspartokinase (AK),[28] glutamate 5-kinase (GK),[29] and *N*-acetyl-L-glutamate kinase (NAGK).[13] The phosphate subdivision consists of uridine monophosphate kinase (UMPK),[30] fosfomycin resistance kinase FomA, and recently discovered isopentenyl phosphate kinase (IPK).[22,31] At the time of initial structural characterization of FomA kinase, NAGK appeared to be the most structurally related homologue. Our predictions of the mechanism of the reaction catalyzed by FomA were made on the basis of a structural comparison with NAGK, which proceeds via a predominantly associative mechanism. The crystal structure of FomA showed preservation of catalytic amino acids of NAGK (K9, K216, and D150 in FomA) as well as good superposition of the phosphate acceptor groups of the substrates. Recently, crystallographic data for IPKs from different organisms have become available: from *Methanocaldococcus jannaschii* (MJ),[22] from *Thermoplasma aciduphilum* (THA),[31] and from *Methanothermobacter thermautotropicus* (MTH).[31] IPKs phosphorylate isopentenyl monophosphate, producing isopentenyl diphosphate, a reaction analogous to that catalyzed by FomA. IPKs exhibit the most structural similarities with FomA, despite a low level of sequence identity to FomA (22–25%), expanding the possibilities for structural comparisons and mechanistic investigations. Structural alignment of FomA with IPKs shows conservation of all previously identified catalytic residues of FomA (K9, K216, and D150) as well as amino acid residues H58 and K18, which have been previously identified in FomA as residues that could be

essential for catalysis. H58 and K18 are invariant in all known FomA and IPK enzymes. Members of the carboxylate subdivision of the AAK superfamily of enzymes lack such equivalent residues in their sequences. In addition, the substrate binding sites (fosfomycin or isopentenyl monophosphate) in all known FomAs and IPKs have invariant S148, D208, T210, and G211 amino acids (FomA amino acid numbering). Such observations strongly support the suggestion that FomA- and IPK-catalyzed reactions proceed via a similar mechanism. In contrast, bacterial UMP kinases, which belong to the last group of the phosphate subdivision of the AAK superfamily of enzymes, share significantly less sequence homology with FomA (19% at the most), nor do they show conservation of the FomA catalytically important amino acids K9 (D, S, or K in UMPKs), K216 (A in UMPKs), and H58 (R in UMPKs); there is no residue equivalent to K18. In terms of quaternary structure, they form stable homohexameric architectures with allosteric regulation, while FomA and IPK enzymes adopt homodimers with no documented allosteric regulation. Hence, the mechanism of phosphorylation by UMPK is likely distinct from that of FomA or IPK enzymes.

ATP Conformation. The ATP conformation is different between two complexes containing the ATP molecule: the ATP·fosfomycin form and the MgATP one. While the ATP conformation in the former structure is basically the same as that observed in the MgAMPPNP·fosfomycin complex, the γ-phosphate of ATP in the latter structure adopts a different orientation, placing the leaving phosphate group closer to the fosfomycin binding site (Figure 3A). The catalytically relevant conformation of ATP is most likely the one observed in the MgATP structure because (1) the MgATP structure contains the catalytic Mg^{2+} cation that binds to ATP and properly orients it for phosphoryl transfer, (2) the γ-phosphoryl group of the ATP molecule is closer to the fosfomycin binding site and is positioned for in-line transfer, (3) there is better superposition between the nucleotides between the MgATP and the structurally homologous *N*-acetyl-L-glutamate and isopentenyl phosphate kinases, and (4) one of the nonbridging O atoms of the γ-phosphoryl group of ATP in the MgATP structure shares almost the same site as one of the O atoms of the phosphate group of the product of the reaction, fosfomycin monophosphate, in the MgADP·FM structure (Figure 3B) or one of the O atoms of the vanadate moiety in the MgADP·$FMVO_3$ structure.

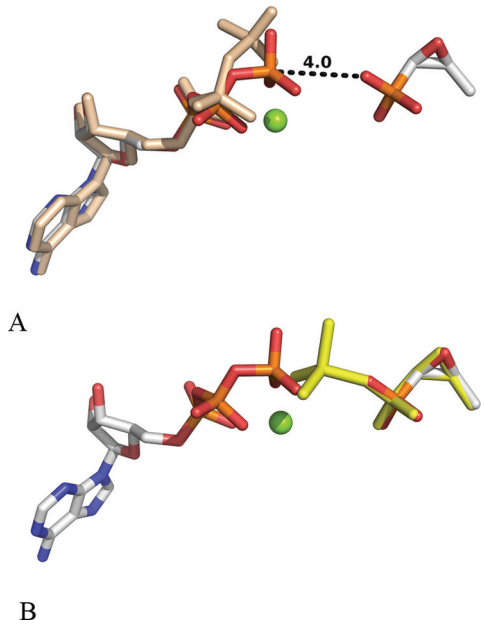

Figure 3. (A) Model of the MgATP·fosfomycin complex based on a superposition of MgATP from the MgATP complex and fosfomycin from the ATP·fosfomycin complex. The attacking oxygen of fosfomycin is 4.0 Å from the γ-phosphorus of ATP. Mg^{2+} is shown as a green sphere. The superimposed ATP molecule from the ATP·fosfomycin complex is colored wheat. (B) Same as panel A with a superposition of fosfomycin monophosphate (yellow).

We built the model of the MgATP·fosfomycin ternary complex using the coordinates of FomA, ATP, and Mg^{2+} from the MgATP complex and the superimposed fosfomycin coordinates from the ATP·fosfomycin structure (Figure 3A). According to the model, the distance between the attacking O atom of fosfomycin and the P atom of the γ-phosphate of ATP is 4.0 Å and the $O_{\beta\gamma}-P_{\gamma}-O_{fos}$ angle is 157.9°.

The MgADP·$FMVO_3$ Complex Mimics the Charge Distribution of the Transition State. Two possible reaction mechanisms are generally described for phosphoryl transfer: an associative mechanism (SN_2-like) or a dissociative mechanism (SN_1-like). The two mechanisms differ in the charge distribution and bond order of the transition state. The SN_2 mechanism is characterized by the formation of the pentacoordinate bipyramidal transition state in which the axial ligands are the nucleophile of the attacking substrate and the bridging oxygen atom between the β- and γ-phosphates. An overall charge distribution for such a transition state is −3. A planar trigonal metaphosphate with an overall charge of −1 is observed for the dissociative mechanism. Hence, the location of positively charged amino acids and the distances from the phosphoryl analogue to the leaving and attacking groups are crucial to distinguish between two possible mechanisms.

Despite our numerous efforts to obtain a pentacoordinate transition state FomA complex, we were able to obtain only a complex in which vanadate is covalently bound to fosfomycin. Formation of such a compound is not unprecedented because monomeric vanadate is known to react readily with phosphate or alkyl phosphate to form phosphovanadate or alkyl phosphovanadate.[32] Fosfomycin vanadate mimics the product of the reaction, fosfomycin monophosphate, rather than the transition state. All the ligands superimpose very well between the MgADP·$FMVO_3$ and MgADP·FM complexes. However, a detailed comparison of two complexes surprisingly reveals many significant differences in terms of protein conformation (Figure 4). The MgADP·$FMVO_3$ complex is the most ordered one among all the FomA crystal structures and the only one that has the ordered so-called "lysine triangle" (K9, K18, and K216). A lysine triangle has been shown to play a catalytic role in isopentenyl phosphate kinases. The MgADP·FM structure has extensive disorder of the loops surrounding the active site, which may indicate that the enzymatic reaction is complete, and the active site loops moved out to allow the product of the reaction, fosfomycin monophosphate, to leave the enzyme active site (Figure 4A,B). In contrast, the active site of the enzyme in the MgADP·$FMVO_3$ complex is closed (Figure 4B). All the loops surrounding the active site are ordered, and the side chain of W202 makes stacking interactions with the adenine ring of ADP. All the amino acids (K9, K18, H58, D208, and T210) that were proposed to play role in the catalytic reaction are ordered in contrast to the MgADP·FM structure in which they are mostly disordered with no electron density at all

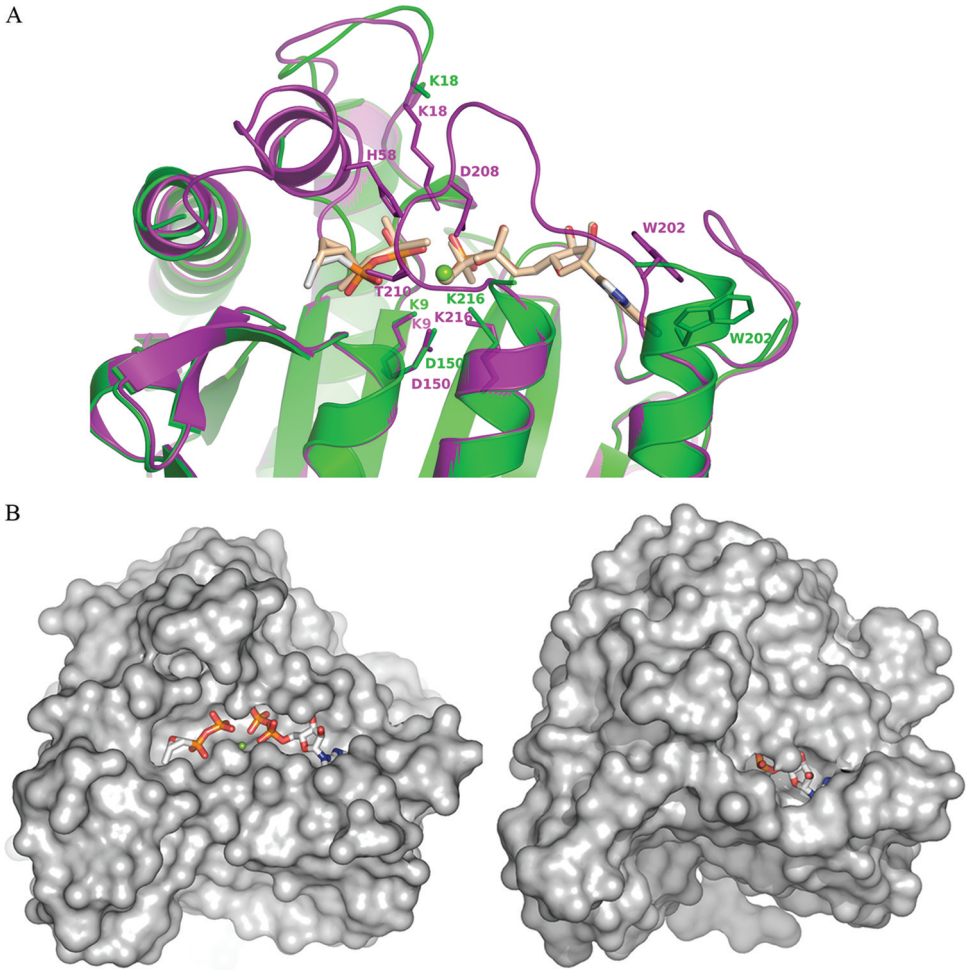

Figure 4. (A) Superposition of the active sites of the MgADP·FM (green) and MgADP·$FMVO_3$ (purple) complexes. Ligand molecules are shown as sticks and Mg^{2+} cations as spheres; ADP and fosfomycin vanadate molecules from the MgADP·$FMVO_3$ complex are colored teal. (B) Surface representation for the MgADP·FM (left) and MgADP·$FMVO_3$ (right) complexes. Ligand molecules (shown as sticks) are exposed to solvent in the former complex, while they are shielded by flexible protein loops in the latter.

(H58, D208, and T210) or with missing electron density for the side chain (K18). There are also differences in the Mg coordination. The MgADP·$FMVO_3$ complex has the Mg cation in a perfect octahedral coordination, while it is only tetracoordinated in the MgADP·FM structure. Such observations and structural differences with the MgATP complex (one of the initial stages of the reaction) in terms of the conformation of the FomA molecule suggest that the conformation of the protein molecule in the MgADP·$FMVO_3$ complex depicts the one between these two stages (before and after catalysis). The ordering of the structure and the locations of several positively charged amino acid residues in the active site close to the vanadate moiety of fosfomycin vanadate suggest that the MgADP·$FMVO_3$ complex approximates the charge distribution in the transition state.

Proposed Enzymatic Mechanism. Taking into account the results of our mutational and structural studies, as well as the sequence conservation in homologous enzymes, we proposed a mechanism of fosfomycin inactivation by FomA protein (Figure 5).

The attacking O atom of fosfomycin is clearly identified. In the model of the MgATP·fosfomycin complex, the angle among this atom, P_γ of ATP, and the bridging $O_{\beta\gamma}$ is 157.9°, which is close for the expected in-line attack on phosphorus with formation of a trigonal bipyramidal transition state. The distance between the attacking O atom of the fosfomycin and the P atom of the γ-phosphate of ATP is 4.0 Å, which is 0.9 Å too short for a dissociative mechanism,[33] suggesting a mechanism with some associative character. Negative charges on ATP are shielded by Mg^{2+}, which ligates all three phosphate groups, by K216, which is H-bonded to the β-phosphate of ATP or ADP in all FomA complexes, and by several positively charged amino acid residues (K9, K18, and H58), which are precisely located around the vanadate moiety of fosfomycin vanadate in the MgADP·$FMVO_3$ complex. Glycine rich loops ^{11}GGSLFS^{16} and ^{53}GGG^{55} may provide additional charge stabilization and function as flexible clamps stabilizing the leaving phosphate and entering phosphonate groups. A high density of positive charges in the phosphoryl transfer site indicates that the transferred phosphate group is highly negatively charged, as would be expected for an associative mechanism. Substrate binding is followed by closure of the active site loops, resulting in ordering and movement of catalytic residues K18, H58, and T210 closer to the midpoint of the phosphoryl transfer site as it is observed in the MgADP·$FMVO_3$ complex, thus participating in transition state stabilization. After phosphoryl transfer is complete, the loops move away to help to release the product of the reaction, fosfomycin monophosphate. Hence, it appears that as in the

dx.doi.org/10.1021/bi2004334 | *Biochemistry* 2011, 50, 6909–6919

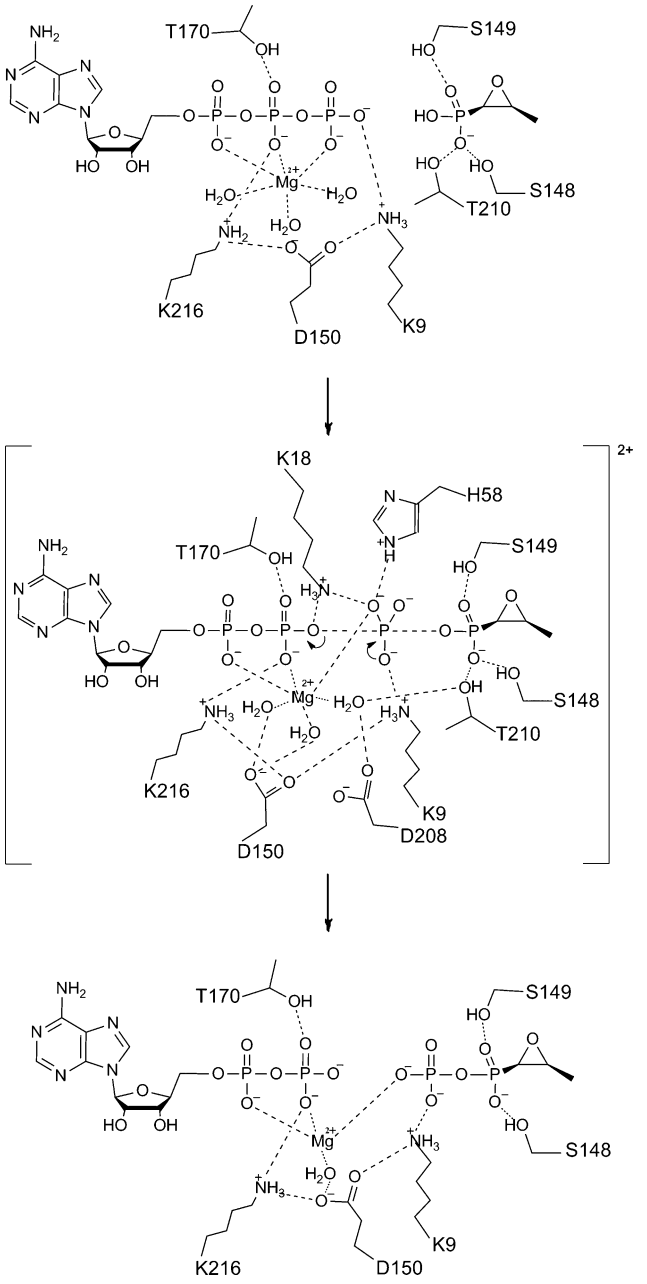

Figure 5. Phosphoryl group transfer in the FomA reaction.

homologous enzymes that also have similarly organized active centers and ternary complexes, FomA-catalyzed phosphoryl transfer takes place by an in-line predominantly associative mechanism.

■ ASSOCIATED CONTENT

Supporting Information

Comparison of protein flexible parts in FomA complexes (Table S1) and SDS−PAGE [10% (w/v) polyacrylamide] gels of purified wild-type and FomA mutant enzyme forms (Figure S1), in which all lanes contain equivalent amounts of protein. This material is available free of charge via the Internet at http://pubs.acs.org.

Accession Codes

The coordinates for the structures reported in this work have been deposited in the Protein Data Bank as entries 3QUN (MgATP complex), 3QUO (ATP·fosfomycin complex), 3QVF (MgADP·$FMVO_3$ complex), 3QUR (MgADP·FM complex), and 3QVH (ADP complex).

■ AUTHOR INFORMATION

Corresponding Author

*E-mail: sveta@lsu.edu. Fax: (225) 578-7258. Telephone: (225) 578-7385.

Funding

Supported by Grant R03 AI074770 from the National Institutes of Health and the Louisiana Governors Biotechnology Initiative.

■ ACKNOWLEDGMENTS

We thank Prof. Tomohisa Kuzuyama (The University of Tokyo) for the sample of fosfomycin monophosphate. Data used in this publication were collected at the Gulf Coast Protein Crystallography Beamline at the Center for Advanced Microstructures and Devices. This beamline is supported by National Science Foundation Grant DBI-9871464, with cofunding from the National Institute for General Medical Sciences. We thank Dr. Henry Bellamy for assistance with data collection.

■ ABBREVIATIONS

AAK, amino acid kinase; NAGK, *N*-acetyl-L-glutamate kinase; AK, N-terminal domain of aspartokinase; CK, carbamate kinase; GK, glutamate 5-kinase; UMPK, uridine monophosphate kinase; IPK, isopentenyl phosphate kinase; NAG, *N*-acetyl-L-glutamate; FM, fosfomycin monophosphate; $FMVO_3$, fosfomycin vanadate; DPO, diphosphate; MJ IPK, *M. jannaschii* isopentenyl phosphate kinase; THA IPK, *T. aciduphilum* isopentenyl phosphate kinase; MTH IPK, *Me. thermautotropicus* isopentenyl phosphate kinase.

■ REFERENCES

(1) Kahan, F. M., Kahan, J. S., Cassidy, P. J., and Kropp, H. (1974) The mechanism of action of fosfomycin (phosphonomycin). *Ann. N.Y. Acad. Sci. 235*, 364−386.

(2) Hendlin, D., Stapley, E. O., Jackson, M., Wallick, H., Miller, A. K., Wolf, F. J., Miller, T. W., Chaiet, L., Kahan, F. M., Foltz, E. L., Woodruff, H. B., Mata, J. M., Hernandez, S., and Mochales, S. (1969) Phosphonomycin, a new antibiotic produced by strains of *Streptomyces*. *Science 166*, 122−123.

(3) Christensen, B. G., Leanza, W. J., Beattie, T. R., Patchett, A. A., Arison, B. H., Ormond, R. E., Kuehl, F. A. Jr., Albers-Schonberg, G., and Jardetzky, O. (1969) Phosphonomycin: Structure and synthesis. *Science 166*, 123−125.

(4) Stein, G. E. (1998) Single-dose treatment of acute cystitis with fosfomycin tromethamine. *Ann. Pharmacother. 32*, 215−219.

(5) Falagas, M. E., Giannopoulou, K. P., Kokolakis, G. N., and Rafailidis, P. I. (2008) Fosfomycin: Use beyond urinary tract and gastrointestinal infections. *Clin. Infect. Dis. 46*, 1069−1077.

(6) Suarez, J. E., and Mendoza, M. C. (1991) Plasmid-encoded fosfomycin resistance. *Antimicrob. Agents Chemother. 35*, 791−795.

(7) Bernat, B. A., Laughlin, L. T., and Armstrong, R. N. (1997) Fosfomycin resistance protein (FosA) is a manganese metalloglutathione transferase related to glyoxalase I and the extradiol dioxygenases. *Biochemistry 36*, 3050−3055.

(8) Cao, M., Bernat, B. A., Wang, Z., Armstrong, R. N., and Helmann, J. D. (2001) FosB, a cysteine-dependent fosfomycin resistance protein under the control of sigma(W), an extracytoplas-

mic-function sigma factor in *Bacillus subtilis*. *J. Bacteriol. 183*, 2380–2383.

(9) Etienne, J., Gerbaud, G., Courvalin, P., and Fleurette, J. (1989) Plasmid-mediated resistance to fosfomycin in *Staphylococcus epidermidis*. *FEMS Microbiol. Lett. 52*, 133–137.

(10) Kobayashi, S., Kuzuyama, T., and Seto, H. (2000) Characterization of the fomA and fomB gene products from *Streptomyces wedmorensis*, which confer fosfomycin resistance on *Escherichia coli*. *Antimicrob. Agents Chemother. 44*, 647–650.

(11) Woodyer, R. D., Shao, Z., Thomas, P. M., Kelleher, N. L., Blodgett, J. A., Metcalf, W. W., van derDonk, W. A., and Zhao, H. (2006) Heterologous production of fosfomycin and identification of the minimal biosynthetic gene cluster. *Chem. Biol. 13*, 1171–1182.

(12) Pakhomova, S., Bartlett, S. G., Augustus, A., Kuzuyama, T., and Newcomer, M. E. (2008) Crystal structure of fosfomycin resistance kinase FomA from *Streptomyces wedmorensis*. *J. Biol. Chem. 283*, 28518–28526.

(13) Ramon-Maiques, S., Marina, A., Gil-Ortiz, F., Fita, I., and Rubio, V. (2002) Structure of acetylglutamate kinase, a key enzyme for arginine biosynthesis and a prototype for the amino acid kinase enzyme family, during catalysis. *Structure 10*, 329–342.

(14) Otwinowski, Z., and Minor, W. (1997) Processing of X-ray diffraction data collected in oscillation mode. *Methods Enzymol. 276*, 307–326.

(15) Bailey, S. (1994) The CCP4 Suite: Programs for Protein Crystallography. *Acta Crystallogr. D50*, 760–763.

(16) Painter, J., and Merritt, E. A. (2006) TLSMD web server for the generation of multi-group TLS models. *J. Appl. Crystallogr. 39*, 109–111.

(17) Howlin, B., Butler, S. A., Moss, D. S., Harris, G. W., and Driessen, H. P. C. (1993) Tlsanl: Tls Parameter-Analysis Program for Segmented Anisotropic Refinement of Macromolecular Structures. *J. Appl. Crystallogr. 26*, 622–624.

(18) Jones, T. A., Zou, J. Y., Cowan, S. W., and Kjeldgaard, M. (1991) Improved methods for building protein models in electron density maps and the location of errors in these models. *Acta Crystallogr. A47* (Part 2), 110–119.

(19) Neau, D. B., Gilbert, N. C., Bartlett, S. G., Boeglin, W., Brash, A. R., and Newcomer, M. E. (2009) The 1.85 Å structure of an 8R-lipoxygenase suggests a general model for lipoxygenase product specificity. *Biochemistry 48*, 7906–7915.

(20) DeLano, W. L. (2002) *The PyMOL Molecular Graphics System*, DeLano Scientific, San Carlos, CA.

(21) Marco-Marin, C., Ramon-Maiques, S., Tavarez, S., and Rubio, V. (2003) Site-directed mutagenesis of *Escherichia coli* acetylglutamate kinase and aspartokinase III probes the catalytic and substrate-binding mechanisms of these amino acid kinase family enzymes and allows three-dimensional modelling of aspartokinase. *J. Mol. Biol. 334*, 459–476.

(22) Dellas, N., and Noel, J. P. (2010) Mutation of archaeal isopentenyl phosphate kinase highlights mechanism and guides phosphorylation of additional isoprenoid monophosphates. *ACS Chem. Biol. 5*, 589–601.

(23) Ramon-Maiques, S., Marina, A., Guinot, A., Gil-Ortiz, F., Uriarte, M., Fita, I., and Rubio, V. (2010) Substrate binding and catalysis in carbamate kinase ascertained by crystallographic and site-directed mutagenesis studies: Movements and significance of a unique globular subdomain of this key enzyme for fermentative ATP production in bacteria. *J. Mol. Biol. 397*, 1261–1275.

(24) Sudom, A. M., Prasad, L., Goldie, H., and Delbaere, L. T. (2001) The phosphoryl-transfer mechanism of *Escherichia coli* phosphoenolpyruvate carboxykinase from the use of AlF_3. *J. Mol. Biol. 314*, 83–92.

(25) Zhou, G., Somasundaram, T., Blanc, E., Parthasarathy, G., Ellington, W. R., and Chapman, M. S. (1998) Transition state structure of arginine kinase: Implications for catalysis of bimolecular reactions. *Proc. Natl. Acad. Sci. U.S.A. 95*, 8449–8454.

(26) Schlichting, I., and Reinstein, J. (1997) Structures of active conformations of UMP kinase from *Dictyostelium discoideum* suggest phosphoryl transfer is associative. *Biochemistry 36*, 9290–9296.

(27) Marina, A., Alzari, P. M., Bravo, J., Uriarte, M., Barcelona, B., Fita, I., and Rubio, V. (1999) Carbamate kinase: New structural machinery for making carbamoyl phosphate, the common precursor of pyrimidines and arginine. *Protein Sci. 8*, 934–940.

(28) Liu, X., Pavlovsky, A. G., and Viola, R. E. (2008) The structural basis for allosteric inhibition of a threonine-sensitive aspartokinase. *J. Biol. Chem. 283*, 16216–16225.

(29) Marco-Marin, C., Gil-Ortiz, F., Perez-Arellano, I., Cervera, J., Fita, I., and Rubio, V. (2007) A novel two-domain architecture within the amino acid kinase enzyme family revealed by the crystal structure of *Escherichia coli* glutamate 5-kinase. *J. Mol. Biol. 367*, 1431–1446.

(30) Marco-Marin, C., Gil-Ortiz, F., and Rubio, V. (2005) The crystal structure of *Pyrococcus furiosus* UMP kinase provides insight into catalysis and regulation in microbial pyrimidine nucleotide biosynthesis. *J. Mol. Biol. 352*, 438–454.

(31) Mabanglo, M. F., Schubert, H. L., Chen, M., Hill, C. P., and Poulter, C. D. (2010) X-ray structures of isopentenyl phosphate kinase. *ACS Chem. Biol. 5*, 517–527.

(32) Tracey, A. S., Willsky, G. R., and Takeuchi, E. (2007) *Vanadium: Chemistry, biochemistry, pharmacology, and practical applications*, CRC Press, Boca Raton, FL.

(33) Mildvan, A. S. (1997) Mechanisms of signaling and related enzymes. *Proteins 29*, 401–416.